Indonesian Journal of Aerospace Vol. 21 No. 2 Desember 2023 : pp 145-162 (Zuhri et al.)
DOI: 10.55981/ijoa.2023.38
https://ejournal.brin.go.id/ijoa/

Correction Maneuver Optimization to Maintain The Local Time of Lapan-A4 Satellite

M. R. Zuhri[1], R. E. Poetro[2], T. Indriyanto[2], L. Faturrohim[2]

[1]Department of Mechanical Engineering, Politeknik Negeri Bandung, Indonesia
[2]Department of Aerospace Engineering, Institut Teknologi Bandung, Indonesia
e-mail: muhammad.rizki@polban.ac.id

Received: 04-05-2023 Accepted: 01-04-2023 Published: 31-12-2023

Abstract

In order for a satellite to achieve a sun-synchronous orbit (SSO), it must have a nodal precession rate equal to the revolution rate of the Earth around the Sun. However, sun-synchronous satellites generally encounter significant perturbations, which lead the local time of the satellite to drift gradually. In this research, the author analyzed potential maneuvers to maintain the local time of an SSO satellite for 5 years of operation of LAPAN-A4 satellite. The analysis was conducted by simulation using GMAT (General Mission & Analysis Tools) software with the LAPAN-A4 satellite as a case study. Furthermore, this research also attempted to find the optimum maneuvering period for each potential maneuver. The results showed that the RAAN correction maneuver is ineffective. It was also found that the most optimum maneuvering plan obtained from this research was a semi-major axis correction maneuver with 4 month maneuvering period with a particular correction targeting strategy.

Keywords: *Sun-synchronous orbit satellite; Correction maneuver; Optimization; LAPAN-A4.*

Nomenclature (Optional)

a	:	Semi major axis	$\boldsymbol{r}$	:	Symmetric correlation matrix	θ	:	True anomaly
e	:	Eccentricity	RAAN	:	Right Ascension of Ascending Node	μ	:	Earth's standard gravitational parameter
EI	:	Expected Improvement	R_E	:	Earth radius	σ	:	variance
$\hat{f}$	:	The prediction of the surrogate model	s	:	Standard deviation	Φ	:	Cumulative distribution function
f_{min}	:	Minimum function value	SMA	:	Semi major axis	ϕ	:	Probability density function
$\boldsymbol{g}$	:	Independent regression basis functions	SSO	:	Sun-synchronous Orbit	Ω	:	RAAN
GMAT	:	General Mission & Analysis Tools	t	:	time	$\dot{\Omega}$	:	Nodal precession rate
i	:	Inclination	x	:	Input of Kriging model	ω	:	Argument of perigee
J_2	:	Earth J_2J_2 perturbation constant	y	:	Output of Kriging model	$_f$	:	Subscript for final variable
LT	:	Local Time	$\boldsymbol{Z}$	:	Gaussian random function	$_0$	:	Subscript for initial value
n	:	Mean motion	$\boldsymbol{\beta}$	:	Regression coefficients			
$\boldsymbol{R}$	:	Correlation function	$\Delta_$	:	Difference			

1. Introduction

Sun-synchronous orbit (SSO) is an orbit that allows a satellite to pass over a region on the Earth's surface at the same local time (LT) every day (Zuhri & Poetro, 2021). It gives several advantages for the operation of an SSO satellite. In terms of schedule, the operator can have a fixed schedule to track the satellite. SSO satellites can also give an advantage for imaging satellites since they will be exposed to roughly the same sunlight proportion every day. Figure 1-1 illustrates the SSO satellites at 3 p.m. local time.

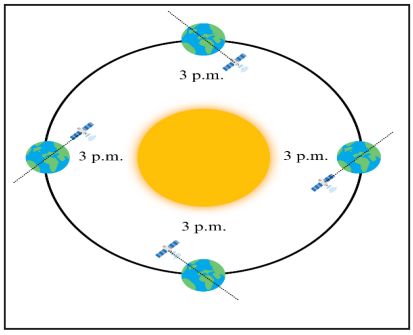

Figure 1-1: SSO satellite illustration.

In order for a satellite to achieve a sun-synchronous orbit (SSO), it must have a nodal precession rate equal to the revolution rate of the Earth towards the Sun, which is 360°/year (Llop et al., 2015). The nodal precession rate, with the J_2 perturbation approach, depends on the semi-major axis, eccentricity, and inclination (Mortari et al., 2004). A combination of these three orbital elements needs to produce, or at least approximate, a nodal precession value of 360°/year continuously. Eq. 1-1 shows the relation of the mean nodal precession rate (Liu et al., 2010) to the three orbital elements by means of J_2 perturbation.

$$\dot{\Omega} = -\frac{3}{2}\frac{R_E^2}{a^2(1-e^2)^2} n J_2 \cos i \qquad (1\text{-}1)$$

Almost all of the SSO satellites currently in orbit have a low orbit altitude (Li & Xu, 2020). As a consequence, the perturbation caused by atmospheric drag and the oblateness of the Earth become significant (Llop et al., 2015). This perturbation gradually leads the orbital element values, including the three aforementioned orbital elements, to change. Hence, the local time of the satellite would change as well. As an example, Figure 1-2 provides a plot of local time drift that occurred to the LAPAN-TUBSAT/A1 satellite, an SSO satellite owned by LAPAN.

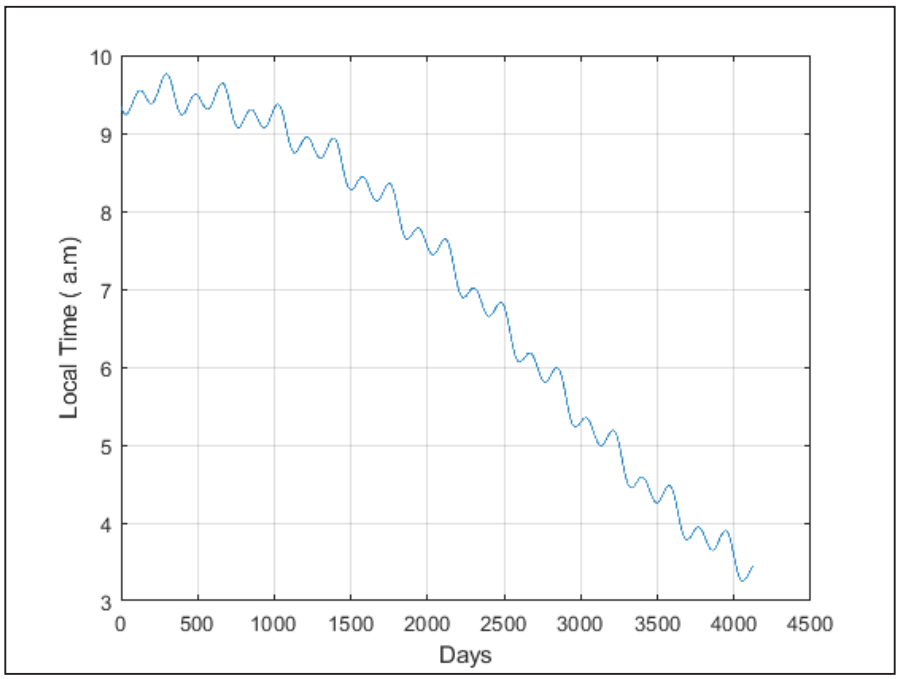

Figure 1-2: LAPAN-TUBSAT/A1 local time drift. (Utama et al., 2018)

If an SSO satellite is left without orbit correction for a long time, the local time drift will be large enough to disrupt the operation and function of the satellite. Therefore, a correction maneuver should be conducted periodically to maintain the local time value to the desired value of 360°/year. KOMPSAT-5, a Korean SSO satellite, performed altitude maneuvers to correct its local time (Lee et al., 2011). GÖKTÜRK satellite from Turkey also adopted the same correction means (Ayan & Akyol, 2019), while China conducted some periodical altitude and/or inclination maneuvers to the FORMOSAT-2 satellite to maintain its sun-synchronous orbit (Chern et al., 2011).

Indonesian National Institute of Aeronautics and Space (LAPAN) previously planned to launch an SSO satellite in the first quarter of 2020 (Utama et al., 2018). Unfortunately, because of COVID-19, the launch was postponed until 2021 (Jemadu, 2020). The satellite, named LAPAN-A4, is an SSO satellite designed to have a propulsion system to perform an orbital maneuver, including the maneuver to maintain the satellite's local time.

In this paper, the authors analyzed correction maneuvers to maintain the local time of the SSO satellite, LAPAN-A4 in this case. Besides analyzing the common SSO maneuvers (i.e., inclination and altitude/semi-major axis maneuvers), the study also evaluated the possibility of a RAAN correction maneuver to maintain the local time of an SSO satellite. The RAAN changes correlate directly with the changes of the satellite's ground-track and hence also correlate with the local time of an SSO satellite.

The study involved a simulation with the LAPAN-A4 satellite as a case study using GMAT (General Mission & Analysis Tools), a spacecraft mission analysis and simulation software developed by NASA. The maneuvering period, the time interval between maneuvers, was also optimized to recommend a maneuvering plan for the five-year operation of the LAPAN-A4 satellite.

2. Methodology

Before conducting a full 5-year-operation simulation of the correction maneuvers, a preliminary calculation was conducted for each maneuvering means (i.e. inclination, semi-major axis, and RAAN correction) to evaluate the effectivity of the maneuvering mean for maintaining the local time of LAPAN-A4 satellite. Only maneuvering means that need fuel consumption below the fuel tank capacity of the LAPAN-A4 satellite were selected to be simulated in a full 5-year operation simulation.

After the evaluation of the maneuvering means effectivity, the selected maneuvering means were simulated in a full 5-year operation simulation in GMAT with a variation of the maneuvering periods, i.e., the time interval between maneuvers. Each maneuvering means

was optimized by analyzing an optimum maneuvering period considering the fuel consumption and the local time drift that occurred as the objective function. The optimization was conducted using a surrogate-based optimization technique via R software. Each optimized maneuvering mean was then compared to give a maneuvering plan recommendation for 5 years operation of the LAPAN-A4 satellite.

This research used the proposed design of the LAPAN-A4 satellite as a case study. Table 2-1 shows the main characteristics of the LAPAN-A4 satellite. LAPAN-A4 satellite has a propulsion system to support correction maneuvers in orbit. The thruster used in this satellite is the 1 N HPGP (High-Performance Green Propulsion) (Utama et al., 2018), a thruster fueled by LMP-103S with a blow-down operation mode developed by ECAPS. Table 2-2 provides the performance of this thruster. For the simplicity of the simulation, the satellite was assumed to bring maximum fuel onboard. It was also assumed that the thrust would be constant throughout the simulation.

Table 2-1. LAPAN-A4 Main Characteristics (Data taken from Ref. (Saifudin et al., 2018)).

Data	Value
Satellite dry mass (kg)	150
Satellite dimension (mm×mm×mm)	744×700×520
Orbit altitude (km)	500
Orbit inclination (deg)	97.38[a]

[a]Decimal values are assumed to provide $\frac{d\Omega}{dt} = 360°/year$

Table 2-2. Thruster Specifications (Data taken from Ref.(Anflo & Möllerberg, 2009; Thomas et al., 2023)).

Data	Value
Tank capacity	4.5 L
Fuel density	1.25 kg/L
Thrust produced	1 N
Feed pressure	2.2 MPa
Blow-down ratio	4:1

2.1. Simulation Scenario

A simulation model to study further the selected maneuvering means was built in GMAT, an open-source trajectory design and optimization software developed by NASA and private industries. GMAT was selected since it is one of the best-tested NASA's open-source software for space mission analysis (Hughes et al., 2014). The built models simulated the operation of the LAPAN-A4 satellite for 5 years, accommodating the correction maneuvers in GMAT with a variation of maneuvering periods. The propagator model for this simulation is JGM-3 with perturbation from the Moon and Sun as point masses.

Maneuvering periods were defined as the time interval between maneuvers. For instance, a 2-months maneuvering period means that the maneuver correction would be performed every 2 months for 5 years of satellite operation. The initial maneuvering periods sampling for this research were chosen to be 1, 2, 3, 4, 5, 6, 10, and 12 months maneuvering period.

(Ruggiero et al., 2011) provided an optimum thrust direction in a function of true anomaly (θ), eccentricity (e), and argument of perigee (ω) for each maneuver. Since the orbit to be simulated is nearly circular, hence the eccentricity was assumed to be zero. Consequently, the optimum thrust direction would be in a direction normal to the orbital plane for inclination and RAAN maneuver. Meanwhile, the optimum thrust direction for semi-major axis maneuver is tangential with the orbit. These optimum thrust directions would then be used for the entire simulation of this paper.

2.1.1. $\dot{\Omega}$ sampling strategy

Due to its oscillation, a strategy for $\dot{\Omega}$ sampling should be established. One way to evaluate the value of $\dot{\Omega}$ is by inspecting the RAAN graph (see Figure 2-1), by assuming that the value of RAAN starts from zero. The RAAN graph is almost linear in the long-term time interval for the LAPAN-A4 case, although still oscillating if we look closely. Therefore, the value of $\dot{\Omega}$ could

be po$\dot{\Omega} = \frac{\Delta\Omega}{\Delta t}$approximated linearly:

However, the trick was the selection of Δt to produce a fine model of $\dot{\Omega}$. If Δt is too large, it would limit the simulation since the $\dot{\Omega}$ value could only be obtained for every Δt interval. If Δt is too small, it is likely to capture the oscillation of the actual $\dot{\Omega}$ which is not favored.

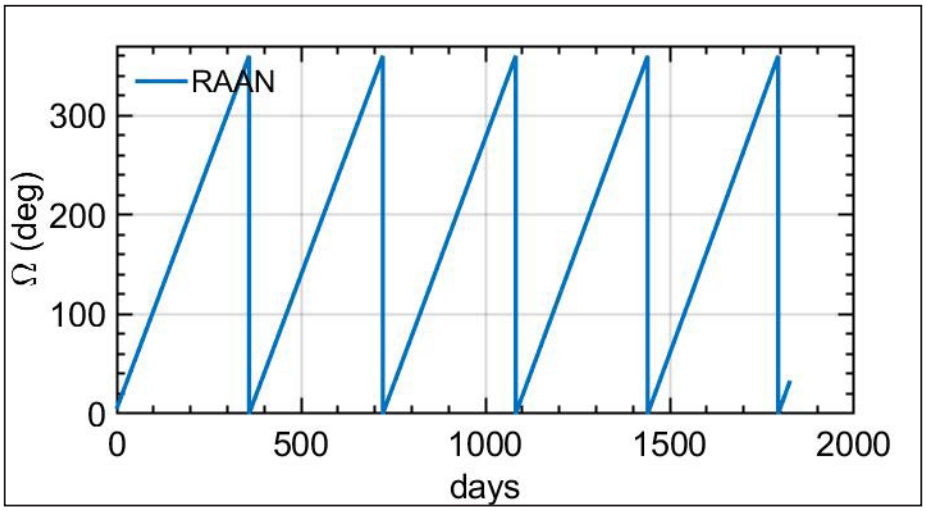

Figure 2-1. RAAN for LAPAN-A4 5-year operation simulation

Some Δt values were evaluated to see the resulting model (see Figure 2-2 – 2-5). The linear model shown as the red line was still capturing the oscillation for small Δt values, such as 7 and 14 days. Along with the increase of the Δt, the oscillation decreased until Δt = 30 days, the linear model gave a result with low oscillation. Hence, this linear sampling method at Δt = 30 days would be used for the complete simulation of inclination and semi-major axis correction maneuvers in the next section.

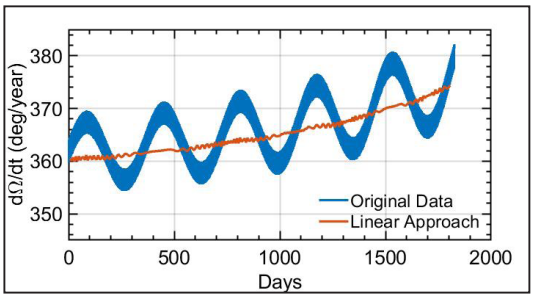

Figure 2-2. $\Delta t = 7\ days$ linear model

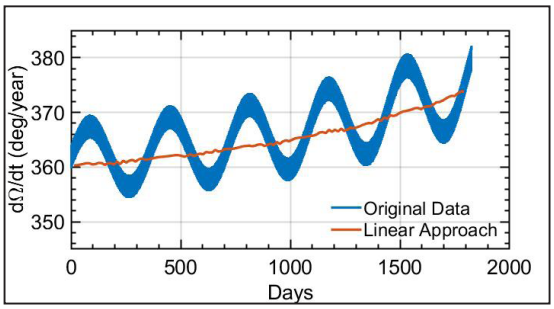

Figure 2-3. $\Delta t = 14\ days$ linear model

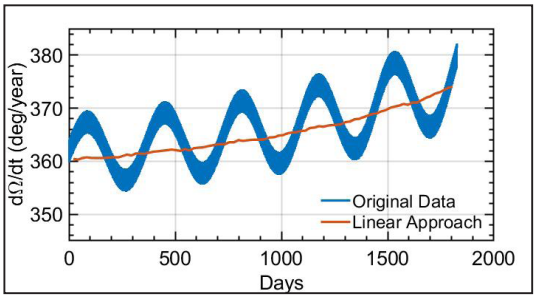

Figure 2-4. $\Delta t = 21\ days$ linear model

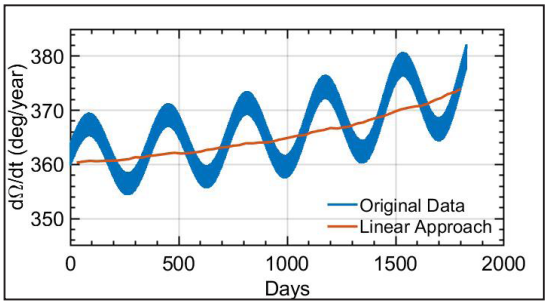

Figure 2-5. $\Delta t = 30\ days$ linear model

2.1.2. Targeting strategy

The maneuvering target could be obtained by modifying Eq. 1-1, by first isolating the term desired to be corrected. For inclination and SMA (semi-major axis) maneuvers, Eq. 1-1 were modified to be, respectively:

$$i = \arccos\left[-\frac{2}{3}\frac{a^2(1-e^2)^2}{R_E^2 n J_2} \times \dot{\Omega}\right] \tag{2-1}$$

$$a = \sqrt[7]{\left(-\frac{3}{2}\frac{1}{\dot{\Omega}} R_E^2 \mu^{\frac{1}{2}} J_2 \cos i\right)^2} \tag{2-2}$$

By defining subscript '0' to be the initial value and 'f' to be the final value, the maneuvering target for inclination ($\Delta i \Delta i$) and SMA ($\Delta a \Delta a$) maneuvers are, respectively:

$$\Delta i = \arccos\left[-\frac{2}{3}\frac{a_f^2\left(1-e_f^2\right)^2}{R_E^2 n_f J_2} \times \dot{\Omega}_f\right] - \arccos\left[-\frac{2}{3}\frac{a_0^2(1-e_0^2)^2}{R_E^2 n_0 J_2} \times \dot{\Omega}_0\right] \tag{2-3}$$

$$\Delta a = \sqrt[7]{\left(-\frac{3}{2}\frac{1}{\dot{\Omega}_f}\frac{R_E^2 \mu^{\frac{1}{2}} J_2 \cos i_f}{\left(1-e_f^2\right)}\right)^2} - \sqrt[7]{\left(-\frac{3}{2}\frac{1}{\dot{\Omega}}\frac{R_E^2 \mu^{\frac{1}{2}} J_2 \cos i_0}{(1-e_0^2)}\right)^2} \tag{2-4}$$

Because the maneuvers usually take a short-period of time, it was assumed that $a_f = a_0$ $a_f = a_0$, $e_f = e_0 e_f = e_0$, $n_f = n_0 n_f = n_0$ for Eq. 2-3 and $i_f = i_0 i_f = i_0$, $e_f = e_0 e_f = e_0$ for Eq. 2-4, the maneuvering target would be:

$$\Delta i = \arccos\left[-\frac{2}{3}\frac{a_0^2(1-e_0^2)^2}{R_E^2 n_0 J_2} \times \dot{\Omega}_f\right] - \arccos\left[-\frac{2}{3}\frac{a_0^2(1-e_0^2)^2}{R_E^2 n_0 J_2} \times \dot{\Omega}_0\right] \tag{2-5}$$

$$\Delta a = \sqrt[7]{\left(-\frac{3}{2}\frac{R_E^2 \mu^{\frac{1}{2}} J_2 \cos i_0}{(1-e_0^2)}\right)^2} \times \left(\frac{1}{\dot{\Omega}_f^{\frac{7}{2}}} - \frac{1}{\dot{\Omega}_0^{\frac{7}{2}}}\right) \tag{2-6}$$

The magnitude of the maneuvering targets for SMA and inclination maneuvers purely depends on the desired final value of the nodal precession rate ($\dot{\Omega}_f \dot{\Omega}_f$). On the other hand, the maneuvering target for the RAAN maneuver is simple since RAAN correlates directly to the local time of the satellite. The maneuvering target for the RAAN maneuver is:

$$\Delta\Omega = \Omega_f(t) - \Omega_0 \tag{2-7}$$

Where $\Omega_f(t)$ is the desired value of RAAN for an SSO satellite at a particular time approximated by $\dot{\Omega} = 360°/\text{year}$.

In the previous work, (Zuhri & Poetro, 2021), the authors set the $\dot{\Omega}_f$ to be 360°/year. The idea was to maintain the value of the nodal precession rate as close as possible to that value so that the local time drift could be damped. Despite being able to lower the maximum local time drift successfully, this strategy had a limitation. This strategy could not lower further the time-history of local time drift because this strategy could only make the slope to be zero ($\dot{\Omega}$ = 360°/year caused the slope of LT drift time-history to be zero).

An alternative targeting strategy to implement and could further lower the local time drift time-history is by setting $\dot{\Omega}_f$ to be lower than 360°/year. The strategy set the final nodal precession rate value to be:

$$\dot{\Omega}_f = 360 - \frac{d\Omega_0 - 0}{X} \tag{2-8}$$

Where $d\Omega_0 d\Omega_0$ is the RAAN deviation before the maneuver is applied, and X is the maneuvering period in years. The term $\frac{d\Omega_0 - 0}{X}$ means that the deviation $d\Omega_0$ that is to be corrected to zero during X period of time. In the next discussions, a targeting strategy expressed by Eq. 2-8 would be denoted as **strategy 2**. On the other hand, the previous targeting strategy, a targeting strategy that intends the final $\dot{\Omega}$ to equal 360°/year, would be denoted as **strategy 1**. Figure 2-6 illustrates both maneuvering target strategies to be employed, while $d\Omega$ is the

deviation of RAAN to the desired value.

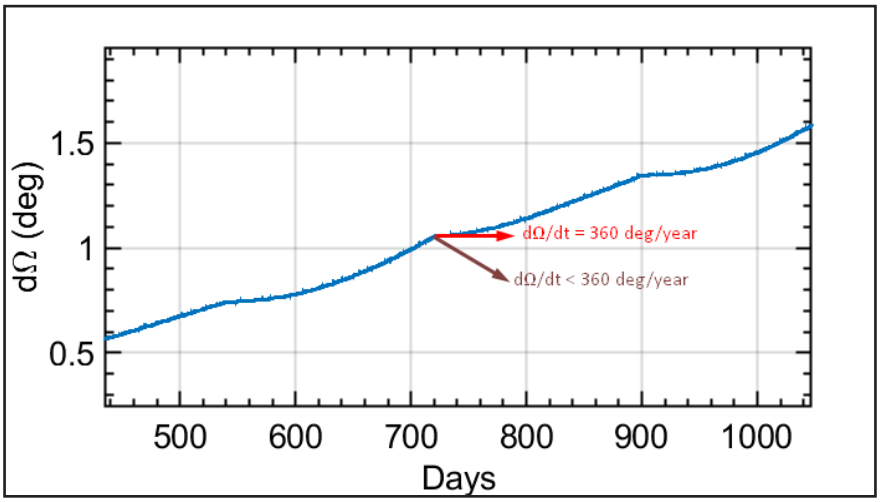

Figure 2-6. Alternative strategy of the maneuvering target illustration

2.2. Surrogate-based Optimization

The maneuvering period optimization was conducted using surrogate-based optimization, also known as metamodel, surrogate, and response surfaces. By definition, this optimization technique approximates the input/output (I/O) function implied by the simulation or experimental model (Kleijnen, 2009). This optimization could be applied either to a deterministic or stochastic model. As implied by (Kleijnen, 2009), examples of deterministic models are given by (Booker et al., 1998) about a helicopter test and by (Gu, 2001) about vehicle safety, while the stochastic model examples are logistic and telecommunication systems modeling.

2.2.1. Surrogate model

There are several models usually used in surrogate-assisted optimization. One of the most promising models is the Kriging model. This model has advantages that it could provide the uncertainty of the prediction model, and it is also very suitable for a complex function (Bartz-Beielstein et al., 2016). Kriging model is also global rather than local (Kleijnen, 2009), so it was used for the model of this optimization.

The Kriging model can be viewed as a global model that combines a local variation (Zhao et al., 2016):

$$y(\boldsymbol{x}) = G(\boldsymbol{x}) + Z(\boldsymbol{x}) \tag{2-9}$$

With x is the input of Kriging Model; $y(\boldsymbol{x})$ is the output of Kriging model; $G(\boldsymbol{x})$ represents the global model of the original function; $Z(\boldsymbol{x})$ stands for the Gaussian random function with zero mean, variance σ^2, and non-zero covariance (Simpson et al., 2001).

The global model is a product of two vectors (Raul & Leifsson, 2021) as follow:

$$G(\boldsymbol{x}) = \boldsymbol{g}^T(\boldsymbol{x})\boldsymbol{\beta} \tag{2-10}$$

where

$$\boldsymbol{g}^T(\boldsymbol{x}) = [g_0(\boldsymbol{x}), g_1(\boldsymbol{x}), g_2(\boldsymbol{x}), \dots, g_{n-1}(\boldsymbol{x})] \tag{2-11}$$

$$\boldsymbol{\beta} = [\beta_0, \beta_1, \beta_2, \dots, \beta_{n-1}]^T \tag{2-12}$$

Are the independent regression basis functions and the regression coefficients respectively, with nn is the number of design variables.

The covariance of $Z(\boldsymbol{x})Z(\boldsymbol{x})$ can be calculated as:

$$Cov[Z(x_i), Z(x_k)] = \sigma^2 R[r(x_j, x_k)] \tag{2-13}$$

Where $j, k = 1, 2, 3, \dots, n_s$ with n_s the number of samples, R represents the correlation

function, and $r(x_j, x_k)$ is the symmetric correlation matrix given as:

$$r(x_j, x_k) = \exp\left[-\sum_{i=1}^{n} \theta_k \left|x_k^i - x_k^j\right|^2\right] \quad (2\text{-}14)$$

Where x_k^i and x_k^j represent the k^{th} components of $\boldsymbol{x}^i$ and $\boldsymbol{x}^j$, and θ_k is the k^{th} component of the unknown correlation parameter consisting $\theta = [\theta_0, \theta_1, \theta_2, \dots, \theta_n]^T$.

As mentioned in (Raul & Leifsson, 2021) by (Simpson et al., 2001), Kriging can also be used to predict the function value at unsampled location $\boldsymbol{x}_u$, named the Kriging predictor $\hat{y}(\boldsymbol{x}_u)$, given as:

$$\hat{y}(\boldsymbol{x}_u) = \boldsymbol{g}^T\hat{\beta} + \boldsymbol{r}^T(\boldsymbol{x}_u)\boldsymbol{R}^{-1}(\boldsymbol{y} - \boldsymbol{G}\hat{\beta}) \quad (2\text{-}15)$$

Where $\boldsymbol{y}$ represents a column vector with length of n_s consisting of the responses of the sample points, $\boldsymbol{r}^T(\boldsymbol{x}_u) = [R(x_u, x_1), R(x_u, x_2), \dots, R(x_u, x_{n_s})]$ stands for the correlation vector between the sample points and the unsampled point of interest, and $\hat{\beta}\hat{\beta}$, as represented in (Raul & Leifsson, 2021) by (Butterfield, 1988), is a maximum likelihood estimation (MLE) of β β expressed as:

$$\hat{\beta} = \frac{\boldsymbol{G}^T\boldsymbol{R}^{-1}\boldsymbol{y}}{\boldsymbol{G}^T\boldsymbol{R}^{-1}\boldsymbol{G}} \quad (2\text{-}16)$$

2.2.2. Infill criteria

The surrogate model built using the Kriging model or prediction is only an approximation of the original function desired to be optimized. The model has a certain accuracy, and it needs to be enhanced to give better optimization results. One way to improve the accuracy of the surrogate model is by adding more points (infill points) in addition to the initial samples.

One kind of infill criterion is the expected improvement (EI). It balances global exploration and local exploitation of the objective function and is proven to be the best route to find the global optimum of a function (Forrester et al., 2008). The typical expression of expected improvement, as provided in (Bhosekar & Ierapetritou, 2018) by (Jones et al., 1998) is:

$$EI(x) = \left(f_{min} - \hat{f}(x)\right)\Phi\left(\frac{f_{min} - \hat{f}(x)}{s}\right) + s\phi\left(\frac{f_{min} - \hat{f}(x)}{s}\right) \quad (2\text{-}17)$$

Where $\Phi(.)$ is the cumulative distribution function; $\phi(.)$ is the probability density function; s is the standard of deviation; f_{min} is the current minimum function value; $\hat{f}$ the prediction of the surrogate model.

In this study, the Kriging model and the expected improvement were used for the surrogate model and the infill criteria, respectively. The surrogate-based optimization conducted in this research flows as follows:

1. Initial data sampling
2. Created the surrogate model based on the initial data sampling
3. Evaluated the infill point from the maximum expected improvement
4. Simulated the infill point in GMAT and extracted the result
5. Updated the current data with the infill point result
6. Repeated from step 2 until the global optimum is found.

3. Preliminary Calculation and Maneuver Potential Evaluation

The preliminary calculation aimed to investigate the effectivity of each correction maneuver to be performed for the LAPAN-A4 satellite. The preliminary calculation involved a rough calculation with certain assumptions and a simulation using GMAT to extract the estimated fuel required for a particular correction maneuver. If the estimation of fuel requirement was lower than the fuel tank capacity of the LAPAN-A4 satellite, that particular correction maneuver would be studied further for simulation of 5 years of operation. Otherwise, if the estimated fuel requirement was far above the fuel tank capacity, that particular correction maneuver would not be studied further.

3.1. Inclination Maneuver Preliminary Calculation

The authors have previously performed a study regarding a maneuvering plan for the LAPAN-A4 satellite using inclination correction maneuvers in (Zuhri & Poetro, 2021) and (Zuhri & Utama, 2021). The research evaluated some maneuvering periods: 2 months, 4 months, 6 months, 12 months, and 24 months. The results showed that the required fuel consumption was still below the maximum fuel capacity of the LAPAN-A4 satellite of 5.6 kg (see Table 3-1). However, that research still has a flaw since it is assumed that the correction target was constant throughout the simulation, as explained previously in section 2.1.1. In fact, the perturbation experienced by the satellite would be different depending on its orbital state, so the correction target for each maneuver should be different. Therefore, further study is required to analyze the inclination maneuver plan for 5 years of operation accommodating a variable correction target by using the sampling strategy provided in section 2.1.1.

Table 3-1. Inclination Maneuver Fuel Consumption from Reference (Zuhri, 2020)

Maneuvering Period	Fuel Consumption [kg]
2 Months	1.889
4 Months	1.902
6 Months	1.944
12 Months	2.090
24 Months	2.521

3.2. Semi-Major Axis Maneuver Preliminary Calculation

The required SMA correction could be obtained by introducing $\dot{\Omega}_f = \dot{\Omega}_0 + \Delta\dot{\Omega}$ to Eq. 3-1, where $\Delta\dot{\Omega}$ is the required change of nodal precession rate, so that:

$$\Delta a = \sqrt[7]{\left(-\frac{3}{2}R_E^2\mu^{\frac{1}{2}}J_2\cos i\right)^2} \times \left(\frac{1}{\left(\dot{\Omega}_0 + \Delta\dot{\Omega}\right)^{\frac{2}{7}}} - \frac{1}{\dot{\Omega}_o^{\frac{2}{7}}}\right) \tag{3-1}$$

The author's previous study (Zuhri & Poetro, 2021) provided data on the required change of nodal precession rate for several maneuvering periods so that the required semi-major axis correction could be calculated using Eq. 3-1 (see Table 3-2). Next, a simulation of SMA maneuver correction was conducted using GMAT to evaluate the required fuel consumption for each maneuvering period. The total required fuel consumption for 5 years of operation was assumed to be only the multiplication of the fuel consumption for one maneuver times the frequency of the maneuver for 5 years of operation. Table 3-3 provides the estimation of the total required fuel for the SMA maneuver for 5 years of operation. The estimation indicated that the required fuel was still below the maximum fuel tank capacity and not too far from the results obtained from the inclination maneuver. Hence, further study is needed to analyze the SMA maneuver to maintain the local time of the LAPAN-A4 satellite.

Table 3-2. Required $\Delta\dot{\Omega}$ from Reference (Zuhri & Poetro, 2021) and Resulting Δa

Maneuvering Period (Months)	Required $\Delta\dot{\Omega}$ (°/year)	Required Δa (km)
2	0.34126	3.199
4	0.68873	6.474
6	1.04241	9.994
12	2.14066	20.517
24	4.50472	43.104

Table 3-3. Total Required Fuel Estimation for SMA Maneuver

Maneuvering Period (Months)	Required Fuel per Maneuver (kg/maneuver)	Total Estimated Required Fuel (kg)
2	0.120	3.600
4	0.244	3.662
6	0.375	3.749
12	0.764	3.819
24	1.591	3.181

3.3. RAAN Maneuver Preliminary Calculation

The required RAAN correction was obtained by calculating the difference between the actual RAAN value and the desired RAAN value for the SSO satellite at a particular moment. The previous study provided some required RAAN correction correlated with appropriate drift after a specific elapsed time, as provided by Table 3-4. By performing a simulation in GMAT, we obtained the required fuel consumption for one maneuver. Furthermore, by assuming that the total fuel consumption is only the multiplication of the fuel consumption for one maneuver times the frequency of the maneuver for 5 years of operation, the total fuel consumption was obtained (see also Table 3-4).

From the results, it is concluded that RAAN correction is not effective for maintaining the local time of the LAPAN-A4 satellite since the total fuel consumption is far from the fuel tank capacity. Since the RAAN correction maneuver directly affects the local time, contrary to the inclination or SMA correction maneuver, which affects the local time indirectly via the nodal precession rate, the correction target for the RAAN correction maneuver is quite large. For comparison, the range of the inclination correction target is between 0.005° - 0.1°, about ten times smaller than the correction target for the RAAN maneuver which is in the range of 0.05° - 1°. This leads the RAAN correction maneuver to be less effective and considerably consume more fuel. Hence, the RAAN correction maneuver was not simulated further in the next section of this paper.

Table 3-4. Total Required Fuel Estimation for RAAN Maneuver

Required RAAN correction (deg)	Correlated with RAAN drift of (days)	Fuel consumption/ maneuver (kg/ maneuver)	Total fuel consumption (kg)
0.05	50	0.259	9.324
0.10	79	0.504	12.096
0.50	273	2.650	15.900
1.00	397	5.350	21.400

3.4. Maneuvering Effectivity Evaluation

From the preliminary calculations above, it was obtained that the only maneuvering means feasible to maintain the local time of the LAPAN-A4 satellite are the semi-major axis correction maneuver and inclination correction maneuver since the total fuel consumption estimations were within the maximum capacity of the fuel tank. On the other hand, the RAAN correction maneuver is not effective to be performed since the total fuel consumption was far beyond the fuel tank capacity and far more consumptive compared to the inclination or SMA correction maneuver. Therefore, in the next phase of this research, the semi-major axis and inclination correction maneuver will be studied further. The study involved a simulation with a variation of the maneuvering period (the time interval between maneuvers) for 5 years of operation. The optimum maneuvering means and maneuvering period were inspected for this LAPAN-A4 satellite case.

4. Simulation Results

4.1. Inclination Correction Maneuver Using Strategy 1

Figures 4-1 and 4-2 respectively show the results of the fuel consumption and the local time drift for various maneuvering periods of inclination maneuver using strategy 1. The results indicated that the simulation has successfully lowered the local time drift which would be around 110 minutes drift if no correction maneuver is performed, as depicted in Figure 4-4. Furthermore, the characteristic of the results is that the shorter the maneuvering period, the less the fuel consumption and the local time drift occurred in general. This phenomenon could happen because the more often the maneuver is performed (i.e. long maneuvering period), the larger the perturbation effects accumulated. Consequently, the maneuvering target would be larger, hence the fuel consumption would be larger, too. A longer maneuvering period also leads the local time to be left rising in a longer time (see Figure 4-2), so the maximum local time drift for a longer maneuvering period would be larger.

By comparing Figure 4-3 and Figure 4-4, it is indicated that the application of $\dot{\Omega}\dot{\Omega}$ sampling strategy elaborated in section 2.1.1 has successfully automated the maneuver for 5 years of operation. The local time drift time-history for this sampling strategy (Figure 4-3) does not show any excessive graph, in contrary to the local time drift time-history obtained from the previous study (see Figure 4-4) which has some excessive graphs (the local time drift becomes below zero).

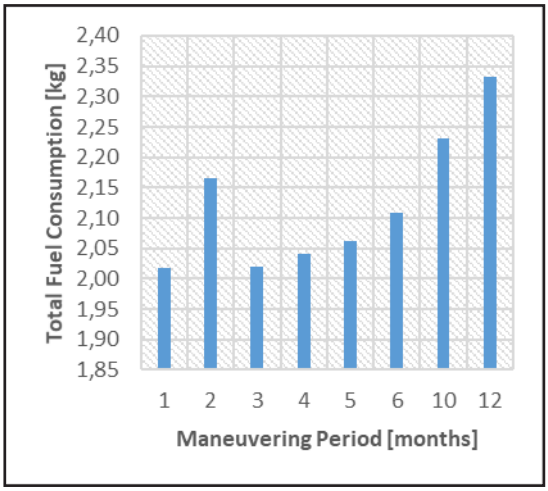

Figure 4-1. Fuel consumption results of inclination maneuver strategy 1

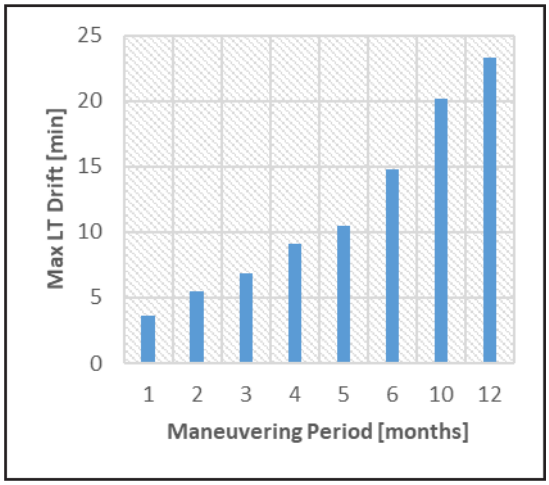

Figure 4-2. Local time drift results of inclination maneuver strategy 1

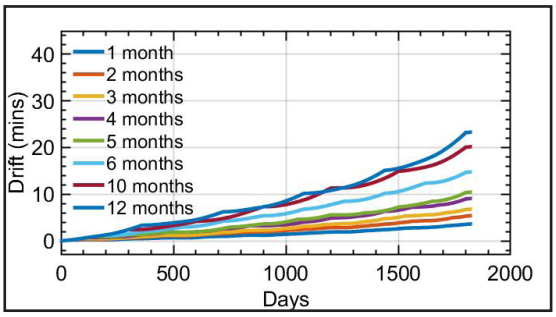

Figure 4-3. Time history of LT drift of inclination maneuver strategy 1

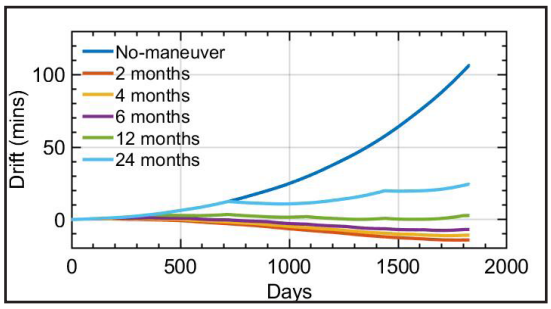

Figure 4-4. Time history of LT drift of inclination maneuver from (Zuhri & Poetro, 2021)

4.2. Semi Major Axis Correction Maneuver Using Strategy 1

Figures 4-5 and 4-6 respectively show the results of fuel consumption and the local time drift for various maneuvering periods of SMA maneuver using strategy 1. This maneuvering mean has also successfully lowered the local time drift, even gives a generally better result compared to inclination correction maneuver. Moreover, besides the maximum local time drift being lower in general, the fuel consumption is also less. The potential reason for this finding is the fact that the SMA maneuver is raising the altitude of the satellite's orbit. Because the

satellite orbit is raised, the dominant perturbation from θatmospheric drag will also be less. Thus, the maneuvering target for the next maneuver would also be less, resulting in a less fuel consumption for 5 years of operation and a smaller maximum local time drift.

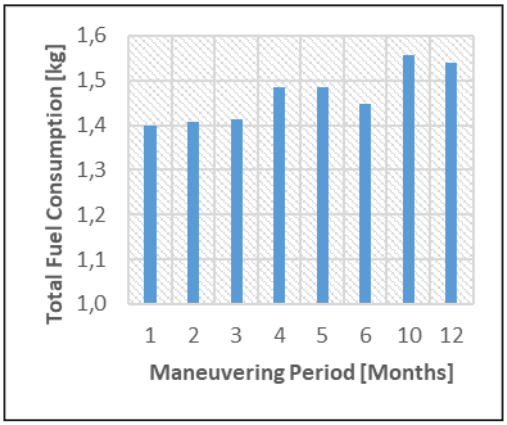

Figure 4-5. Fuel consumption results of SMA maneuver strategy 1

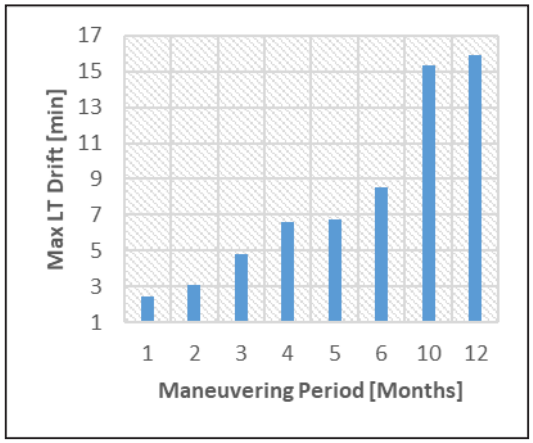

Figure 4-6. Local time drift results of SMA maneuver strategy 1

4.3. Inclination Correction Maneuver Using Strategy 2

Figures 4-7 and 4-8 show the fuel consumption and maximum local time drift results of inclination correction maneuver using strategy 2 compared to the results using strategy 1. The use of strategy 2 has successfully lowered further the maximum local time drift for all maneuvering periods as suggested in Figure 4-8. However, as a drawback, fuel consumption is higher in general. It does make sense because strategy 2 yields a larger maneuvering target. Moreover, the use of strategy 2 for maneuvering target also leads the fuel consumption and maximum local time drift results to be more fluctuating towards maneuvering period, in contrary to strategy 1 which is more in order. This is caused by the presence of some excessive maneuvers that lowered the local time drift excessively to negative value instead of lowering the local time drift to be zero, especially for low maneuvering period (see Figure 4-9).

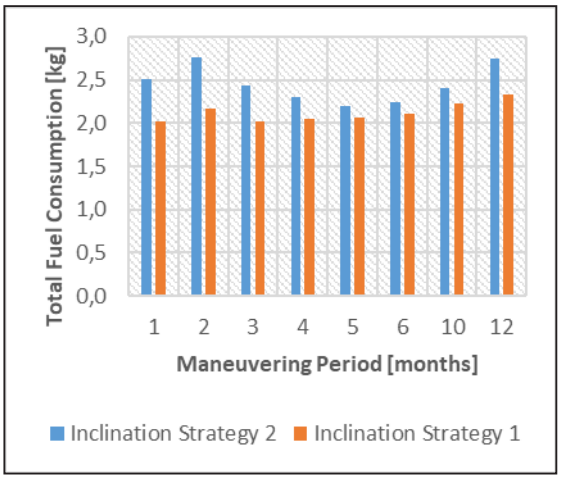

Figure 4-7. Fuel consumption results of inclination maneuver strategy 2

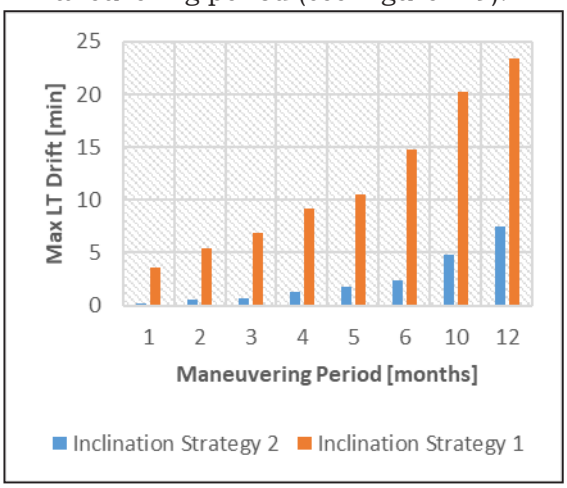

Figure 4-8. Local time drift results of inclination maneuver strategy 2

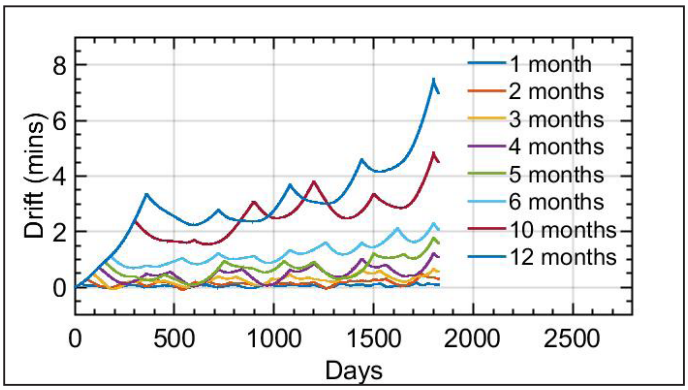

Figure 4-9. LT drift time history of inclination maneuver using strategy 2

4.4. Semi Major Axis Correction Maneuver Using Strategy 2

Figures 4-10 and 4-11 show the fuel consumption and maximum local time drift results of SMA correction maneuver using strategy 2 compared to the results using strategy 1. The same as the results of inclination maneuver using strategy 2, SMA maneuver using strategy 2 has successfully lowered the maximum local time drift for all maneuvering periods compared to strategy 1 as shown in Figure 4-10. However, as a consequence, the fuel consumption results are generally higher since the implementation of strategy 2 leads to a larger maneuvering target. Additionally, the use of strategy 2 for maneuvering target also yields the fuel consumption and maximum local time drift results to be more fluctuating in respect to the maneuvering periods, contrary to strategy 1. The reason for this is the presence of some excessive maneuvers that lowered the local time drift excessively. The local time drift which was previously intended to be close to zero, quite the opposite became negative (see Figure 4-11).

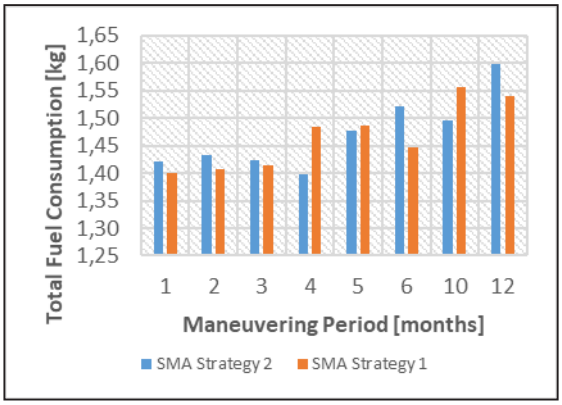

Figure 4-10. Fuel consumption results of SMA maneuver strategy 2

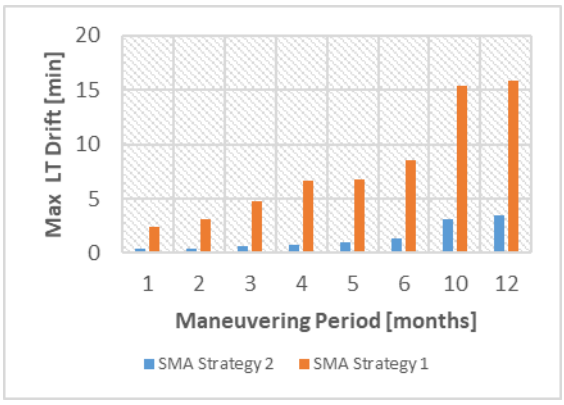

Figure 4-11. Local time drift results of SMA maneuver strategy 2

5. Optimization Results

Figure 5-1 – 5-4 show the results of the optimization for 4 simulated maneuver types: inclination and SMA correction maneuver with 2 variations of targeting strategy (strategy 1 and strategy 2). The white dots represent the initial data sampling; the black dots represent the current optimum value of the surrogate model; and the red dots represent the minimum of inverse of expected improvement. The initial data sampling was all the same: 1, 2, 3, 4, 5, 6, 10, and 12 months maneuvering period, whereas the number of infill points was different depending on the iteration process. From the results, the optimization only succeeded to find an optimum maneuvering period for inclination correction maneuver using strategy 2.

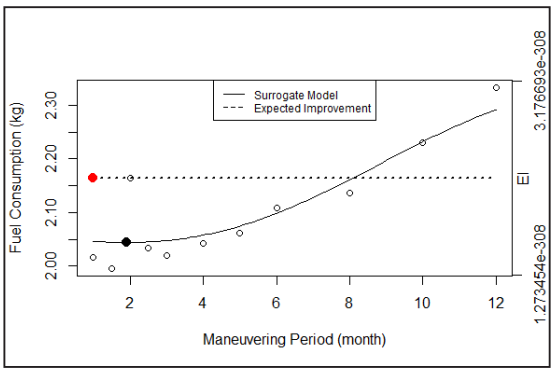

Figure 5-1. Optimization result for inclination correction maneuver using strategy 1

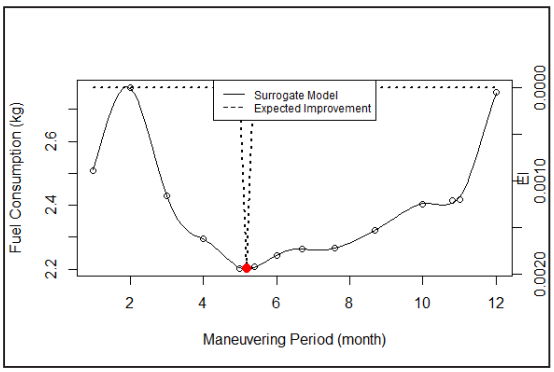

Figure 5-2. Optimization result for inclination correction maneuver using strategy 2

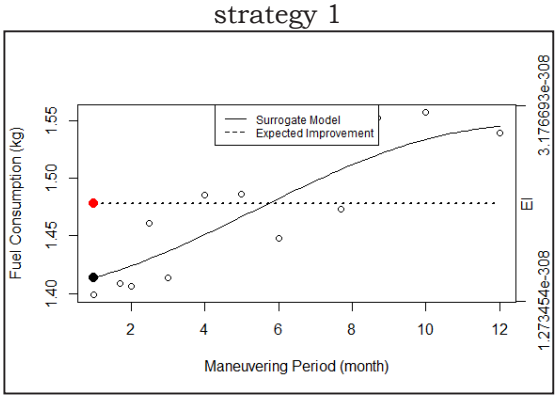

Figure 5-3. Optimization result for SMA correction maneuver using strategy 1

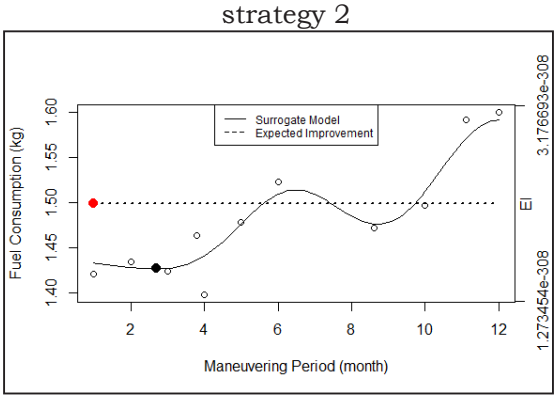

Figure 5-4. Optimization result for SMA correction maneuver using strategy 2

For the optimization result of the inclination correction maneuver using strategy 1, the iteration process is stuck at the third iteration. The expected improvement became a plateau; hence, the next infill point could not be decided. This result could happen as a result of the presence of data that was very far from the model predicted by the kriging model, which was the 2-month maneuvering period data. The Kriging model predicted that the 2-month maneuvering period data should be at the lower value, but the actual data of the 2-month maneuvering period were at the upper value. Consequently, the Kriging model could not give an appropriate model and the optimum value could not be obtained.

Similar to the result from the inclination correction maneuver using strategy 1, the optimization result from the SMA correction maneuver using both strategies stuck as the expected improvement plot became a plateau. The result from the SMA correction maneuver using strategy 1 was too fluctuating, while the result from the SMA correction maneuver using strategy 2 had data that was far from the predicted model (4-month maneuvering period). As a results, the Kriging model was not able to give proper models and the optimum values could not be extracted from these maneuver types.

Although the optimization technique could not find the global optimum value of some maneuver types, we were still able to inspect the local optimum value by simply comparing all of the results as it is. Table 5-1 provides the optimum maneuvering period for each maneuver type. From the results, the SMA correction maneuver using strategy 2 with 4-month maneuvering period was selected to be the optimum maneuvering plan since it gives the least fuel consumption. The minimum fuel consumption would impact the launch cost of the LAPAN-A4 satellite. Besides the fuel price is considerably expensive, minimizing the fuel consumption would also lead to the decrease in the satellite's total mass. Since the launch cost of the LAPAN-A4 satellite depends on the mass of the satellite, the minimum fuel consumption would

also lower the launch cost of the satellite.

Table 5-1. Optimum maneuvering period for each maneuver type

Maneuver type	Optimum maneuvering period (months)	Fuel Consumption (kg)
Inclination strategy 1	1.5	1.996 kg
Inclination strategy 2	5.2	2.123 kg
SMA strategy 1	1	1.399 kg
SMA strategy 2	4	1.398 kg

Besides the fact that the SMA correction maneuver using strategy 2 with a 4-months maneuvering period leads to minimum fuel consumption, it also gives operational advantages to the LAPAN-A4 satellite. The maximum local time drift of this maneuver is only 0.74 minutes, which is so low that the imaging function of the satellite will be optimum. Additionally, the maneuvering period is large enough so that the maneuver scheduling will be easier because the maneuvers are only performed every 4 months.

There is still a possibility of the presence of the more optimum maneuvering period than the results mentioned above. From the results, only one maneuver type had been successfully optimized. The rest maneuver types were not successfully optimized, so the optimum maneuvering period for each of these maneuvers was only selected among the available data. One way to improve the optimization result of these maneuvers is by inspecting a narrower interval in which the expected optimum value stands. In this way, the possibility of finding the optimum maneuvering period for each maneuver type will be higher.

The simulation limitation that emerged as a consequence of the Δt = 30 days selection (see section 4.1) also leads to a possibility of a more optimum maneuvering period. The Δt selection caused the maneuvering period to be 1 month at a minimum. However, if we see the trend, the fuel consumption for each maneuver type tends to be less for the lower maneuvering period.

6. Conclusion

From the preliminary evaluation of this research, it was concluded that the RAAN correction maneuver was not feasible since the fuel requirement exceeded the maximum fuel tank capacity of the LAPAN-A4 satellite. In contrast, the inclination and SMA correction maneuvers could still be performed to maintain the local time of the LAPAN-A4 satellite. However, the SMA correction maneuver is generally better than the inclination correction maneuver because it gave lower maximum local time drift results with less fuel consumption.

The most optimum maneuver obtained from this research is the SMA correction maneuver using strategy 2 with a 4-months maneuvering period since it resulted in the lowest fuel consumption of 1.398 kg. Moreover, it also has operational advantages because the maneuver is only performed every 4 months, which is arguably not too frequent.

There is still a possibility to have a more optimum maneuvering period. From the results, 3 maneuver types were not successfully optimized, so the optimum maneuvering period for each of these maneuvers was only selected among the available data. One way to improve the optimization result of these maneuvers is by inspecting a narrower interval in which the expected optimum value stands. In addition, the Δt selection caused the maneuvering period to be 1 month at a minimum. Even though, if we see the trend, the fuel consumption for each maneuver type tends to be less for the lower maneuvering period.

Acknowledgements

The authors would like to thank the Department of Mechanical Engineering Polban and Department of Aerospace Engineering ITB for the support on this research.

Contributorship Statement

MRZ and LF Developed the simulation and analyzed the results, REP and TI analyzed the results.

References

Anflo, K., & Möllerberg, R. (2009). Flight demonstration of new thruster and green propellant technology on the PRISMA satellite. *Acta Astronautica*, *65*(9–10). https://doi.org/10.1016/j.actaastro.2009.03.056

Ayan, A., & Akyol, A. (2019). In-plane and out of plane maneuvers in GÖKTÜRK operations. *Proceedings of 9th International Conference on Recent Advances in Space Technologies, RAST 2019*. https://doi.org/10.1109/RAST.2019.8767897

Bartz-Beielstein, T., Naujoks, B., Stork, J., & Zaefferer, M. (2016). *Tutorial on surrogate-assisted modelling*.

Bhosekar, A., & Ierapetritou, M. (2018). Advances in surrogate based modeling, feasibility analysis, and optimization: A review. In *Computers and Chemical Engineering* (Vol. 108). https://doi.org/10.1016/j.compchemeng.2017.09.017

Booker, A. J., Dennis, J. E., Frank, P. D., Serafini, D. B., & Torczon, V. (1998). Optimization Using Surrogate Objectives on a Helicopter Test Example. In *Computational Methods for Optimal Design and Control*. https://doi.org/10.1007/978-1-4612-1780-0_3

Butterfield, C. P. (1988). Aerodynamic pressure and flow-visualization measurement from a rotating wind turbine blade. *American Society of Mechanical Engineers, Solar Energy Division (Publication) SED*, *7*.

Chern, J. S., Lin, S. F., & Wu, A. M. (2011). Orbital maneuver and keeping of FORMOSAT-2. *Acta Astronautica*, *68*(7–8). https://doi.org/10.1016/j.actaastro.2010.09.018

Forrester, A. I. J., Sóbester, A., & Keane, A. J. (2008). Engineering Design via Surrogate Modelling. In *Engineering Design via Surrogate Modelling*. https://doi.org/10.1002/9780470770801

Gu, L. (2001). A comparison of polynomial based regression models in vehicle safety analysis. *Proceedings of the ASME Design Engineering Technical Conference*, *2*. https://doi.org/10.1115/detc2001/dac-21063

Hughes, S. P., Qureshi, R. H., Cooley, D. S., Parker, J. J. K., & Grubb, T. G. (2014). Verification and validation of the general mission analysis tool (GMAT). *AIAA/AAS Astrodynamics Specialist Conference 2014*. https://doi.org/10.2514/6.2014-4151

Jemadu, L. (2020, October). Peluncuran Satelit LAPAN-A4 Diundur ke 2021. Retrieved from Suara.com: https://suara.com

Jones, D. R., Schonlau, M., & Welch, W. J. (1998). Efficient Global Optimization of Expensive Black-Box Functions. *Journal of Global Optimization*, *13*(4). https://doi.org/10.1023/A:1008306431147

Kleijnen, J. P. C. (2009). Kriging metamodeling in simulation: A review. In *European Journal of Operational Research* (Vol. 192, Issue 3). https://doi.org/10.1016/j.ejor.2007.10.013

Lee, B. S., Hwang, Y., Jung, O. C., & Yoon, J. C. (2011). Orbit maintenance for calibration of KOMPSAT-5. *2011 3rd International Asia-Pacific Conference on Synthetic Aperture Radar, APSAR 2011*.

Li, C., & Xu, B. (2020). Optimal scheduling of multiple Sun-synchronous orbit satellites refueling. *Advances in Space Research*, *66*(2). https://doi.org/10.1016/j.asr.2020.03.049

Liu, X., Baoyin, H., & Ma, X. (2010). Five special types of orbits around mars. *Journal of Guidance, Control, and Dynamics*, *33*(4). https://doi.org/10.2514/1.48706

Llop, J. V., Roberts, P. C. E., Palmer, K., Hobbs, S., & Kingston, J. (2015). Descending sun-synchronous orbits with aerodynamic inclination correction. *Journal of Guidance, Control, and Dynamics*, *38*(5). https://doi.org/10.2514/1.G000183

Mortari, D., Wilkins, M., & Bruccoleri, C. (2004). On Sun-Synchronous Orbits and Associated Constellations. *Paper of the 6-Th Dynamics …*, *January*.

Raul, V., & Leifsson, L. (2021). Surrogate-based aerodynamic shape optimization for delaying airfoil dynamic stall using Kriging regression and infill criteria. *Aerospace Science and Technology*, *111*. https://doi.org/10.1016/j.ast.2021.106555

Ruggiero, A., Pergola, P., Marcuccio, S., & Andrenucci, M. (2011). Low-Thrust Maneuvers for the Efficient Correction of Orbital Elements. *32nd International Electric Propulsion Conference*.

Saifudin, M. A., Karim, A., & Mujtahid. (2018). LAPAN-A4 Concept and Design for Earth Observation and Maritime Monitoring Missions. *ICARES 2018 - Proceedings of the 2018 IEEE International Conference on Aerospace Electronics and Remote Sensing Technology*. https://doi.org/10.1109/ICARES.2018.8547143

Simpson, T. W., Peplinski, J. D., Koch, P. N., & Allen, J. K. (2001). Metamodels for computer-based engineering design: Survey and recommendations. In *Engineering with Computers* (Vol. 17, Issue 2). https://doi.org/10.1007/PL00007198

Thomas, J. C., Rodriguez, F. A., Teitge, D. S., & Petersen, E. L. (2023). Lab-scale ballistic and safety property investigations of LMP-103S. *Combustion and Flame*, *253*. https://doi.org/10.1016/j.combustflame.2023.112810

Utama, S., Saifudin, M. A., & Mukhayadi, M. (2018). A Green Propulsion System Requirement for LAPAN-A4. *ICARES 2018 - Proceedings of the 2018 IEEE International Conference on Aerospace Electronics and Remote Sensing Technology*. https://doi.org/10.1109/ICARES.2018.8547078

Zhao, Y., Lu, W., & Xiao, C. (2016). A Kriging surrogate model coupled in simulation-optimization approach for identifying release history of groundwater sources. *Journal of Contaminant Hydrology*, *185–186*. https://doi.org/10.1016/j.jconhyd.2016.01.004

Zuhri, M. R., & Poetro, R. E. (2021). Station-Keeping Simulation and Planning for LAPAN-A4 Satellite Using Finite-Burn Thruster. *Jurnal Teknologi Dirgantara*, *19*(1), 57–66.

Zuhri, M. R., & Utama, S. (2021). Inclination maneuver simulation with non-impulsive thruster for Sun-synchronous satellite. *AIP Conference Proceedings*, *2366*. https://doi.org/10.1063/5.0060159